Food & Function

ROYAL SOCIETY OF CHEMISTRY

PAPER

View Article Online
View Journal | View Issue

Cite this: *Food Funct.*, 2024, **15**, 809

Preparation of microgels loaded with lycopene/NMN and their protective mechanism against acute liver injury

Jian Ge, *† Luting Ye,† Min Cheng,† Weijia Xu, Zhaowen Chen and Feng Guan

This study aimed to enhance the stability and bioavailability of lycopene (LYC) and nicotinamide mononucleotide (NMN) by incorporating them into porous microgels after loading LYC into liposomes. The particle size, zeta potential, encapsulation rate (%), scanning electron microscopy images, and stability and release kinetics characteristics in simulating digestion confirmed that the microgels had high LYC and NMN encapsulation rates (99.11% ± 0.12% and 68.98% ± 0.26%, respectively) and good stability and release characteristics. The protective effect and potential mechanism of microgels loaded with LYC and NMN on lipopolysaccharide (LPS)-induced acute liver injury in C57BL/6 mice were investigated by intragastric administration for 28 days prior to LPS exposure. The results showed that the microgels loaded with LYC and NMN significantly ameliorated LPS-induced liver injury and reduced the inflammatory response and oxidative stress. In addition, LYC and NMN can not only act on the Toll-like receptor 4 (TLR4)/MD2 complex but also regulate TLR4-related miRNAs (miR-145a-5p and miR-217-5p) in serum extracellular vesicles, thereby synergistically inhibiting the TLR4/NF-κB signaling pathway. In addition, the microgels loaded with LYC and NMN were able to enrich beneficial bacteria that produced short-chain fatty acids and reduce harmful bacteria. In conclusion, LYC and NMN protected against LPS-induced acute liver injury *via* inhibition of oxidative stress and inflammation, as well as regulating the gut microbiota.

Received 18th August 2023,
Accepted 2nd December 2023

DOI: 10.1039/d3fo03293k

rsc.li/food-function

Introduction

The liver is an important metabolic organ in the body. Gut-derived toxins ingested in the body can hinder liver metabolism and cause damage. When the gut microbiota is disturbed, a large amount of endotoxin leaks from the intestine to the liver through the portal vein, also causing liver injury through inflammation, oxidative stress, and liver necrosis.[1] A single intraperitoneal injection of lipopolysaccharide (LPS), as a unique component in the outer membrane of Gram-negative bacteria, is the most commonly used model reagent to simulate acute injury caused by bacterial infection and external stimulation.[2]

Lycopene (LYC) is a natural lipid-soluble pigment abundant in fruits and vegetables.[3] The rich conjugated double bonds in the structure enable it to capture peroxide free radicals or quench singlet oxygen.[4] LYC can also promote the activation of nuclear factor erythroid 2-related factor 2 (Nrf2) to regulate antioxidant enzymes and thus enhance the antioxidant defense system *in vivo*.[5] In addition, LYC can inhibit the secretion of inflammatory factors and reduce the inflammatory response by preventing the activation of nuclear factor kappa-B (NF-κB) and downregulating the expression of cyclooxygenase-2 (COX-2).[6] However, LYC may show poor stability, by undergoing processes such as *cis–trans* isomerism and oxidative degradation, at any time due to various environmental factors. Moreover, due to poor water solubility and low intestinal permeability, the bioavailability of LYC is only 0.1%–1.6%.[7]

Nicotinamide mononucleotide (NMN) is a water-soluble natural bioactive nucleotide with α and β isomers,[8] of which the latter is an active form. At present, the biological function of NMN has not been fully discovered. However, as the most direct complementary precursor of NAD^+, NMN was proven to rely on its transformation into NAD^+ to exhibit antioxidant and anti-inflammatory effects through various mechanisms. First, NAD^+ can inhibit the production of ROS, thus preventing oxidative stress and inflammation.[9] Second, NAD^+ is a dependent substrate for many important enzymes. Some researchers found that the activity of silencing information regulator 2-related enzyme-1 (SIRT1), whose deacetylation can regulate

College of Life Sciences, China Jiliang University, 258 XueYuan Street, XiaSha Higher Education Zone, Hangzhou, 310018 Zhejiang Province, People's Republic of China.
E-mail: ge103640427@163.com
† These authors contributed equally to this work.

various transcription factors, including Nrf2 and NF-κB, increases after NMN supplementation.[10] In addition, as an important hydrogen-transmitting co-enzyme in cells, NAD^+ is a key signaling molecule that controls cell function and survival.[11]

Microgels are a class of network structure polymers formed by the crosslinking of bio-polymer molecules under various forces, such as covalent, hydrogen, and ionic bonds. They have high packing capacity owing to their large specific surface area and high porosity. Microgels can improve not only the stability of substances but also target release to increase bioavailability.[12] Proanthocyanidins from Bayberry (*Myrica rubra Sieb. Et Zucc.*) leaves (BLPs) and chitosan (CS) are two kinds of polymer materials widely used in the food industry. BLP is a good natural antioxidant,[13] and CS can prolong the interaction time and increase the transmembrane absorption of substances through electrostatic force with the cell membrane.[14] Microgels prepared with CS and BLP can play a role in slowly releasing and reducing the oxidative degradation of encapsulation under the premise of safety and nontoxicity.

In this study, LYC was encapsulated by liposomes and a microgel bilayer structure to improve its stability and bioavailability. Using liposomes and microgels as carriers, a coexisting system of lipid-soluble (LYC) and water-soluble (NMN) functional active substances was constructed. An acute liver–intestinal model of mice was established by LPS induction, and the protective effects and mechanisms of LYC and NMN on inflammation and oxidative stress were further studied.

Materials and methods

Materials and reagents

CS (deacetylation > 75%) and LPS (from *E. coli* O55:B5) were provided by Sigma–Aldrich (St Louis, MO, USA). LYC (purity of 80%) and NMN (purity of 95%) were obtained from Shanghai Yuanye Biotechnology Co., Ltd (Shanghai, China).

Preparation of liposomes and microgels

Liposomes containing LYC (LYC-LPs) were prepared by a thin-film ultrasound method.[15] Soybean phospholipids (Shanghai Taiwei Pharmaceutical Co., Ltd, Shanghai, China), cholesterol (Shanghai Adamas Reagent Co., Ltd, Shanghai, China), and LYC were dissolved in chloroform. The organic solvent was evaporated by rotary evaporation to form a homogeneous film, which was then dispersed with 0.05 M phosphate buffered saline (PBS). LYC-LP was obtained by probe ultrasonic homogenization in an ice bath for 5 min (100 W, 5 s each time, 5 s intermittently) and filled with nitrogen for closed storage.

CS was completely dissolved in 1% acetic acid solution, and LYC-LP and NMN solutions were added to the CS solution drop by drop under the conditions of magnetic agitation. In the laboratory, BLP was extracted in the early stage and separated by using a Sephadex LH-20 column to obtain BLP with an average polymerization degree of 3.53. The BLP solution was carefully added to the above mixed solution, and the mixture was thoroughly stirred until it was evenly mixed to obtain an LYC-loaded microgel (CS-LYC-BLP), NMN-loaded microgel (CS-NMN-BLP), and LYC and NMN co-loaded microgel (CS-LYC/NMN-BLP).[16]

Particle size and zeta potential

Distilled water was used as the dispersion medium, and 1 mL of the 500-fold diluted sample was added to the sample cell of zeta sizer Nano ZS90 (Malvern Instruments Co., Ltd, Malvern, UK) to determine the particle size and zeta potential.

Encapsulation efficiency

Free LYC was extracted with hexane[17] and centrifuged at 3000 rpm for 5 min. The extract was dried with N_2 and redissolved in the mobile phase containing 10% chloroform. The content of free LYC was detected by HPLC.

The content of free NMN was determined by an ultrafiltration centrifugal method. The microgel was placed into an ultrafiltration centrifugal tube with an interception molecular weight of 3000 and centrifuged at 4000*g* for 30 min. The content of NMN in the filtrate was detected by HPLC.

$$\text{Encapsulation} = \frac{m_0 - m_1}{m_0} \times 100\%$$

where m_0 is the total content of LYC or NMN, and m_1 is the free content of LYC or NMN.

Stability under different influencing factors

CS-LYC-BLP was exposed to 2500 Lux light, metal ions (Cu^{2+} and Fe^{3+}), or oxygen. The LYC retention content was detected at 2, 4, 8, 12, and 24 h separately. The protective effect of the microgel on the stability of LYC was investigated using LYC solution and LYC-LP as the controls.

CS-NMN-BLP was exposed to different pH levels (pH 3.0, 5.0, 9.0, and 11.0) and temperatures (40 °C, 60 °C, and 80 °C). The sampling conditions were consistent with those of LYC, and NMN solution was used as the control.

Simulated gastrointestinal digestion *in vitro*

The simulated gastric fluid (SGF) contained 2 g L^{-1} NaCl and 3.2 g L^{-1} pepsin (1 : 3000, Beijing Solarbio Technology Co., Ltd, Beijing, China), and the pH was adjusted to 2.0 with HCl. The simulated small intestinal fluid (SIF) was composed of 6.8 g L^{-1} KH_2PO_4, 5 mmol L^{-1} $CaCl_2$, 10 g L^{-1} trypsin (1 : 250, Shanghai Yuanye Biotechnology Co., Ltd, Shanghai, China), and 5 mg mL^{-1} porcine bile salt (Beijing Solarbio Technology Co., Ltd, Beijing, China). The pH was adjusted to 7.5 with 0.2 mol L^{-1} NaOH.[18]

The sample was mixed with SGF at a ratio of 1 : 1, and simulated digestion was carried out at 100 rpm at 37 °C. After 2 h of gastric digestion, the enzyme was inactivated, and $NaHCO_3$ was added to adjust the pH to 7.0. An equal-volume SIF was added for 2 h of intestinal digestion. The digestive stability was examined every 0.5 h.

The content of LYC release was determined by extraction with hexane. Samples were mixed with SGF or SIF, and simu-

lated release was performed at 100 rpm at 37 °C. Samples were taken at 0.25, 0.5, 1, 2, and 4 h, and an equal amount of blank medium was supplemented. The release of NMN was investigated by dialysis.[19] The samples were mixed with SGF or SIF into a dialysis tube, placed in the release medium with the pH levels 2.0 and 7.5, and released under the same conditions as above.

$$\text{Cumulative release rate} = \frac{\sum_{i-t}^{i=t-1} c_i V_i + c_t V_t}{m} \times 100\%$$

where c_i and c_t are free concentrations at the i and t times of sampling, respectively; V_i and V_t are the i and t sampling volumes, respectively; and m is the total amount.

Appearance observation through SEM

A small amount of freeze-dried sample was dipped on the sample table with a double-sided conductive adhesive and gilded by sputter coating. The micromorphology of the samples was analyzed by scanning electron microscopy (SEM) under high vacuum at an accelerating voltage of 3 kV.

Animal experiments

Healthy 8-week-old male C57BL/6J mice (20 ± 2 g) with SPF (Special Pathogen Free) grade were purchased from SLACK Laboratory Animal Co., Ltd (Shanghai, China), with the animal qualification certificate number (Shanghai) 2022-0004. The environment was guaranteed to be suitable for temperature and humidity, and the mice were kept under an alternating day/night cycle (12 h/12 h). During the experiment, the mice were not restricted from drinking clean water and eating feed. All animal experiment programs were performed in accordance with the Guidelines for Care and Use of Laboratory Animals of China Jiliang University and approved by the Laboratory Animal Ethics Committee (2023-003) of China Jiliang University (Hangzhou, China). The ingredients of mouse feed are shown in Table 1.

After 1 week of adaptive feeding, the C57BL/6 mice were randomly divided into six groups. The control group and model group were gavaged with normal saline daily, and the CS-BLP group was gavaged with a blank microgel. According to the literature,[20,21] the CS-LYC-BLP group was gavaged with a LYC-loaded microgel containing 10 mg kg^{-1} LYC, the CS-NMN-BLP group was gavaged with a NMN-loaded microgel containing 100 mg kg^{-1} NMN, and the CS-LYC/NMN-BLP group was gavaged with a LYC and NMN co-loaded microgel containing 5 mg kg^{-1} LYC and 50 mg kg^{-1} NMN. And the LYC and NMN concentrations were converted and calculated according to their purities (%). After 28 days of treatment, the control group was intraperitoneally injected with the same amount of PBS, whereas the other groups were treated with 10 mg kg^{-1} LPS.[22] The mice were sacrificed after 12 h, and the serum, liver tissue, and cecum contents were collected. The serum inflammatory factors and tissue oxidative stress levels of the mice were detected in accordance with the requirements of the corresponding kit. The liver tissue was fixed in 10% formalin, dehydrated, embedded in paraffin, and stained with hematoxylin–eosin (H&E).

Table 1 Nutrient composition of mouse feed

Raw material	Proportioning (g kg^{-1})
Corn	280
Flour	360
Soybean meal	160
Fish meal	50
Soybean	25
Soybean oil	22
Yeast powder	8
Alfalfa powder	5
Bran	30
Premix	60

Real-time quantitative PCR (RT-PCR) analysis

In accordance with the instructions of a TRIzol Plus RNA Purification kit and SuperScript III First-Strand Synthesis SuperMix kit, total RNA was extracted from the liver, and cDNA was synthesized by reverse transcription. RT-PCR was conducted to determine the expressions of Sirt1 and Toll-like receptor 4 (TLR4) in the liver. The quantitative PCR primers were designed using Primer Premier 6.0 and Beacon designer 7.8 software. They were synthesized by Shenggong Bioengineering Co., Ltd (Shanghai, China). The primer sequences are shown in Table 2. RT-PCR was performed using the PowerUp™ SYBR™ Green Master Mix (Applied Biosystems, Foster City, CA, USA) that was programmed for denaturation at 95 °C for 60 s, followed by 40 cycles of 95 °C for 15 s and 63 °C for 25 s. Relative expressions levels of target genes were normalized to GAPDH, evaluated by the $2^{-\Delta\Delta Ct}$ method and given as a ratio to control in the experiment.

Western blotting

Completely broken liver tissues were cleaved on ice and centrifuged for protein extraction. The total protein concentration was determined using a BCA quantitative kit. The extracted total protein was separated by SDS-PAGE and transferred to a PVDF membrane. The membrane was sealed with T-TBS (containing 5% BSA) at room temperature for 1 h and then rinsed with T-TBS three times. The corresponding primary antibodies were added: rabbit anti-NF-κB p65 (1 : 1000, CST 8242, Boston, USA), anti-p-p65 (1 : 1,000, CST 3033, Boston, USA), anti-Nrf2 (1 : 500, Thermo Fisher PA5-88084, Waltham, MA, USA), anti-p-Nrf2 (1 : 1000, Thermo Fisher PA5-67520, Waltham, MA, USA), and anti-GAPDH (1 : 1000, Abcam ab181602, Cambridge, UK). They were used as internal parameters and incubated overnight at 4 °C. After the membranes were rinsed with T-TBS, they were incubated with a HRP-conjugated goat anti-mouse IgG secondary antibody (1 : 5000, Thermo Pierce 31160, Waltham, MA, USA) and a goat anti-rabbit IgG secondary antibody (1 : 5000, Thermo Pierce 31210, Waltham, MA, USA) at room temperature for 1 h. Protein expression was visualized on X-ray films by following the instructions of the SuperSignal West Dura Extended Duration Substrate (Thermo Pierce,

Table 2 Real-time PCR primers in the mouse liver

Gene	GenBank accession number	Reverse transcription primer sequences (5′ → 3′)	Size (bp)
Mouse GAPDH	GU_214026.1	GAAGGTCGGTGTGAACGGATTTG CATGTAGACCATGTAGTTGAGGTCA	127
Mouse Sirt1	NM_019812.3	GGGAACCTTTGCCTCATCTACATT CACCACCTAGCCTATGACACA	90
Mouse TLR4	NM_021297.2	GGCATGGCATGGCTTACACCA GAGAGGCCAATTTTGTCTCCACA	134

Waltham, MA, USA). ImageJ software was used to analyze the optical density of bands to calculate the relative protein expression.

Isolation and characterization of serum extracellular vehicles (EVs)

Ultrafast centrifugation was applied to extract serum EVs. The serum was centrifuged at 10 000 rpm for 30 min, and the precipitation was discarded. The supernatant was transferred to a Beckman L-100XP super-centrifuge (Brea, CA, USA) at 100 000*g* for 2 h, and then the supernatant was aspirated and abandoned. The precipitates were centrifuged again at 100 000*g* for 2 h after being washed and suspended with PBS. Subsequently, the supernatant was abandoned, and the precipitates were resuspended with 200 μl of PBS to obtain EVs. Quantification was performed using a BCA kit (Thermo Fisher Ltd, Waltham, MA, USA). The EVs were characterized using transmission electron microscopy (TEM, HT7700, Hitachi Instruments Co., Ltd, Shanghai, China). The average particle size of the EVs was detected using a Flow NanoAnalyzer N30E (Xiamen Fuliu Biological Technology Co., Ltd, Xiamen, China). EV-labeled proteins tetraspanins (CD9 and CD63) and endosome or membrane-binding proteins (TSG101) were detected by western blotting.

miRNA prediction

miRNAs in mammals exert post-transcriptional regulation by binding to the 3′ UTR region of the transcript sequence. Therefore, TargetScan (**https://www.targetscan.org/vert**) and miRanda (**https://www.microrna.org**) were used to predict TLR4 as the miRNA target gene. First, all miRNAs related to TLR4 in mice were analyzed on miRDB. They were input into TargetScanMouse for further verification to ensure reliability of the results. Finally, miR-145a-5p and miR-217-5p were screened for possible interactions with TLR4.

MiRNA levels in EVs detected by RT-qPCR

MiRNAs were extracted from EVs in accordance with the instructions of a PureLink miRNA Isolation Kit and a SuperScript III Reverse Transcriptase kit, and the reverse transcribed miRNA stem ring primer sequences are shown in the Table 3. The expression levels of miR-145a-5p and miR-217-5p in the mouse serum exosomes in each group were detected by RT-qPCR. The RT-qPCR primer sequence is shown in Table 4.

Double luciferase assay

To verify the interaction of TLR4 3′ UTR fragments with miR-217-5p putative binding sites, the pmirGLO vector with TLR4 3′ UTR WT or MUT was constructed. 293T cells were seeded in a 96-well plate at a density of 1×10^5 cells per well. After 24 h, the pmirGLO vector, miR-217-5p mimics and the corresponding controls (miRNA-NC) were co-transfected into the 293T cells. After 48 h of transfection, Firefly and Renilla luciferase activities were sequentially measured using the Dual Glo Luciferase Assay system (Promega Co., Ltd, USA).

Molecular docking

Considering NMN plays a functional activity in the form of NAD^+ after absorption in the body, molecular docking was used to simulate the interaction of LYC and NAD^+ with a TLR4–MD2 protein complex.[23] The three-dimensional structure of LYC was obtained from the TCMSP database (no. 10267-310), and that of the TLR4–MD2 protein complex was obtained from the PDB protein database (no. 2Z65). The three-dimensional structure of NAD^+ was obtained using alcohol dehydrogenase from a *Drosophila lebanonensis* binary complex with NAD^+ (no. 1B14), and then excess enzymes and small molecules were removed. The molecular docking operations were as follows: before docking, PYMOL was used to remove excess proteins and small molecules in the structure, and then the AutoDockTools version 1.5.7 program was used to remove H_2O, hydrogenation, *etc*., set a ligand, detect the twist key, and the file was saved in the pdbqt format. Docking was performed using AutoDock version 4.2.6, and the docking number was set to 50.

Gut microbiota composition analysis

Microbial DNA was extracted from the mouse cecal samples in accordance with the instructions of the FastLee DNA kit for feces (Hangzhou Legenomics Bio-Pharm Technology Co., Ltd, Hangzhou, China). The V3–V5 region of the bacterial 16S ribosomal RNA gene was amplified using primers 515 F (5′-GTGCCAGCMGCCGCGG-3′) and 907 R (5′-CCGTCAATTCMTTTRAGTTT-3′). Then, the amplicon library was paired-end sequenced (2 × 250) on an Illumina Novaseq platform (Mingke Biotechnology (Hangzhou) Co., Ltd) in accordance with the standard protocols.

Statistical analysis

Statistical comparisons were analyzed by one-way ANOVA followed by Duncan's *post hoc* test using SPSS version 18.0. All

Table 3 Reverse transcription primer sequences of miRNAs

Gene	GenBank accession number	Reverse transcription primer sequences (5′ → 3′)
mmu-miR-145a-5p-RT	MIMAT0000157	GTCGTATCCAGTGCAGGGTCCGAGGTATTCGCACTGGATACGACAGGGAT
mmu-miR-217-5p-RT	MIMAT0000679	GTCGTATCCAGTGCAGGGTCCGAGGTATTCGCACTGGATACGACTCCAGT
U6	M10329.1	GTCGTATCCAGTGCAGGGTCCGAGGTATTCGCACTGGATACGACGTCATCC

Table 4 Real-time PCR primers of miRNAs

Gene	Forward primer and universal primer (5′ to 3′)
mmu-miR-145a-5p-F	CGGTCCAGTTTTCCCAGGAA
mmu-miR-217-5p-F	CGCGTACTGCATCAGGAACTG
U6-F	CGCTTCGGCAGCACATATACTAA
Universal reverse primer (micro-R)	AGTGCAGGGTCCGAGGTATT

differences were regarded as significant at $P < 0.05$. Data were shown as mean ± standard deviation (SD).

Result

Particle size, zeta potential and encapsulation efficiency

As shown in Table 5, the encapsulation efficiency of LYC by liposomes was 60.37%, which was further improved after microgel re-encapsulation. The average encapsulation efficiencies of LYC by CS-LYC-BLP and CS-LYC/NMN-BLP were 99.20% and 99.11%, respectively, and those of NMN by CS-NMN-BLP and CS-LYC/NMN-BLP were 66.80% and 68.98%, respectively. Meanwhile, the particle size and zeta potential of LYC-LP were 404.8 nm and +4.75 mV, respectively. The average particle sizes of CS-LYC-BLP, CS-NMN-BLP, and CS-LYC/NMN-BLP were 1490, 1668.33, and 1218.33 nm, respectively; their average zeta potentials were −30.93, −30.03, and −29.47 mV, respectively. When the absolute value of zeta potential reached 30, the system was considered stable. The values of microgels were all close to or greater than 30, indicating that the systems were stable.

Microgels significantly increased the stability of LYC and NMN

The LYC in solution had the worst stability. Specifically, under the influence of light and metal ions, it was completely lost within 24 h. In addition, the retention rate was only 20% after 24 h of exposure to oxygen. After the encapsulation treatment with liposomes, the LYC retention rate increased after 24 h of exposure to various influencing factors. The microgel further improved the stability of LYC, and the retention rate of LYC under various influencing factors reached more than 50% after 24 h (Fig. 1).

The stability of NMN was relatively stable at 40 °C, but it worsened with the increase in temperature. When the temperature reached 80 °C, the NMN in solution and microgel completely degraded within 12 h. Under heating conditions, the microgels did not significantly protect the stability of NMN. In addition, NMN was decreased in acidic or alkaline environments but markedly ameliorated after microgel encapsulation (Fig. 2).

Table 5 Characterization of liposomes and microgels

Sample	Encapsulation efficiency (%)		Particle size/nm	Zeta potential/mV
	LYC	NMN		
LYC-LP	60.37 ± 0.14	—	404.8 ± 22.58	4.75 ± 0.11
CS-LYC-BLP	99.20 ± 0.09	—	1490 ± 134.26	−30.93 ± 1.21
CS-NMN-BLP	—	66.80 ± 0.61	1668.33 ± 164.10	−30.03 ± 2.60
CS-LYC/NMN-BLP	99.11 ± 0.12	68.98 ± 0.26	1218.33 ± 77.78	−29.47 ± 0.23

Simulating gastrointestinal digestion and *in vitro* release

LYC was significantly degraded in SGF, but it remained stable in SIF. After *in vitro* gastrointestinal simulation digestion for 4 h, the retention rates of LYC in CS-LYC-BLP and CS-LYC/NMN-BLP were 53.52% and 60.84%, respectively (Fig. 3A). However, NMN was relatively stable in the gastrointestinal digestion stage. Although a small amount of degradation was observed in SGF, NMN still had more than 80% retention rate after 4 h of gastrointestinal simulated digestion (Fig. 3B).

LYC was released in SGF at a lower rate (<20%) and a higher rate in SIF (Fig. 4A). However, the release characteristic of NMN was different from that of LYC, which showed continuous release, with release rates of more than 80% in SGF or SIF (Fig. 4B).

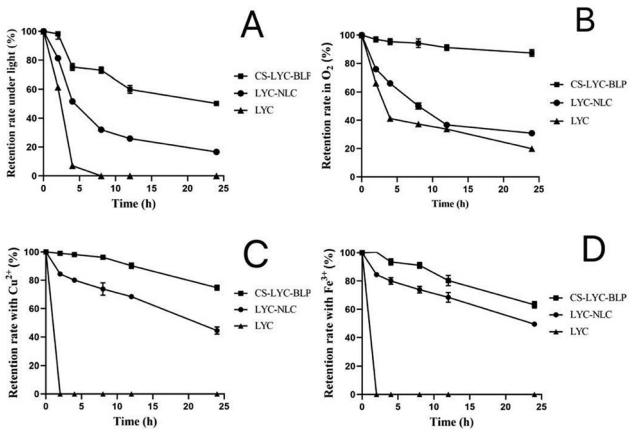

Fig. 1 Stability of LYC under different influencing factors. (A) Stability of LYC under light, (B) oxygen, (C) Cu^{2+}, and (D) Fe^{3+}. Note: CS-LYC-BLP: lycopene-loaded microgel, LYC: lycopene.

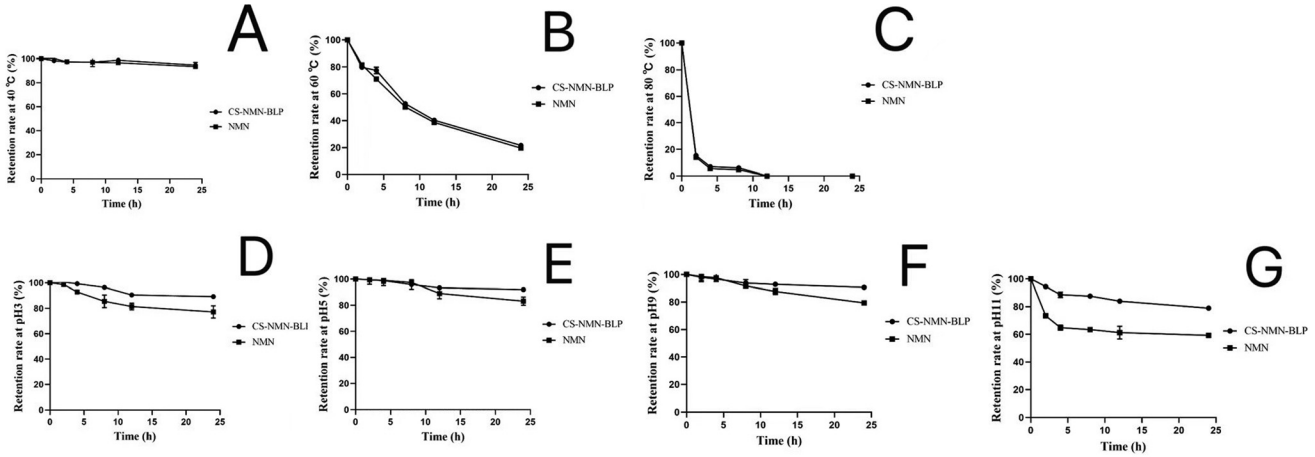

Fig. 2 Stability of NMN under different influencing factors. Stability of NMN to temperatures of (A) 40 °C, (B) 60 °C, and (C) 80 °C and to pH levels of (D) 3.0, (E) 5.0, (F) 9.0, and (G) 11.0. Note: CS-NMN-BLP: nicotinamide mononucleotide-loaded microgel, NMN: nicotinamide mononucleotide.

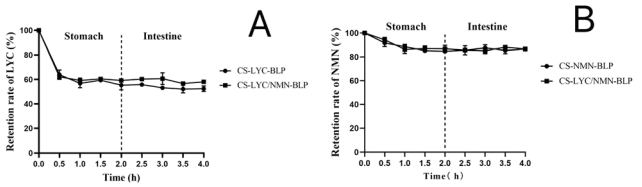

Fig. 3 Simulated gastrointestinal digestion *in vitro*: (A) LYC and (B) NMN. Note: CS-LYC-BLP: lycopene-loaded microgel, CS-LYC/NMN-BLP: lycopene and nicotinamide mononucleotide co-loaded microgel, CS-NMN-BLP: nicotinamide mononucleotide-loaded microgel.

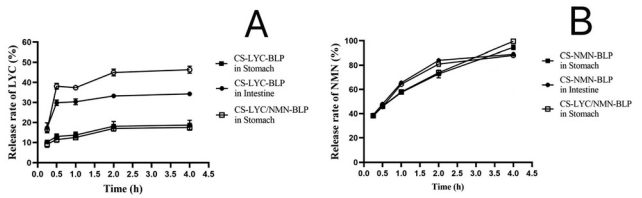

Fig. 4 Simulated gastrointestinal release *in vitro*: (A) LYC and (B) NMN. Note: CS-LYC-BLP: lycopene-loaded microgel, CS-LYC/NMN-BLP: lycopene and nicotinamide mononucleotide co-loaded microgel, CS-NMN-BLP: nicotinamide mononucleotide-loaded microgel.

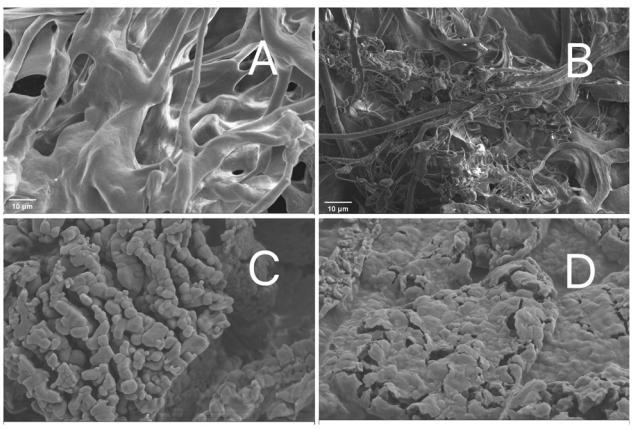

Fig. 5 Appearance observation by SEM: (A) CS, (B) CS-BLP, (C) LYC-LP, and (D) CS-LYC/NMN-BLP. The red arrows pointed to a porous, spongy structure (A), more filamentous antennae (B), enlarged particles (C) and filled cavities (D), respectively.

Appearance observation

The overall structure of the macromolecular crosslinking was observed at ×1000 magnification. The freeze-dried CS samples showed a porous, spongy structure (Fig. 5A), and more filamentous antennae adhesions appeared after BLP was added (Fig. 5B). The existence of LYC-LP and NMN in CS-LYC/NMN-BLP was clearly observed at ×10 000 magnification. Most LYC-LP showed a spheroid or ellipsoidal shape with uniform size, and a few liposomes adhered to one another, resulting in enlarged particles (Fig. 5C). Moreover, fewer pores were found in CS-LYC/NMN-BLP (Fig. 5D), indicating that LYC-LP and NMN entered the pores of the microgel and filled the cavities in its structure.

Obvious reduction in serum inflammatory cytokines in LPS-induced mice by microgels loaded with LYC and NMN

The obtained results showed that the serum levels of TNF-α, IL-6, and IL-1β in the model and CS-BLP groups significantly increased ($P < 0.05$) compared with those in the control group, indicating that LPS promoted the secretion of inflammatory factors in serum. As expected, the inhibitory effects on inflammatory cytokines in LPS-induced mice were demonstrated in the CS-LYC-BLP, CS-NMN-BLP, and CS-LYC/NMN-BLP groups (Fig. 6).

Significant alleviation in LPS-induced oxidative stress levels in the liver by microgels loaded with LYC and NMN

The MDA levels and the GSH-px and SOD activities were measured to investigate the effect of LYC and NMN on LPS-

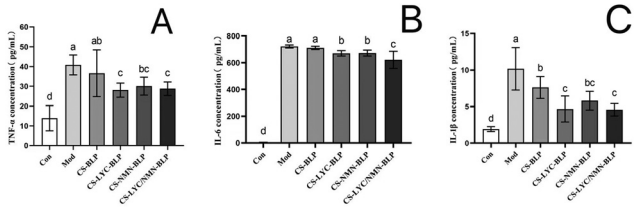

Fig. 6 Levels of inflammatory cytokines in serum. (A) Level of TNF-α in serum. (B) Level of IL-6 in serum. (C) Level of IL-1β in serum. No significant difference between groups is represented by the same letter ($P > 0.05$), and significant difference is represented by different letters ($P < 0.05$). Note: CS-BLP: chitosan and proanthocyanidins from Bayberry leaves, CS-LYC-BLP: lycopene-loaded microgel, CS-NMN-BLP: nicotinamide mononucleotide-loaded microgel, CS-LYC/NMN-BLP: lycopene and nicotinamide mononucleotide co-loaded microgel.

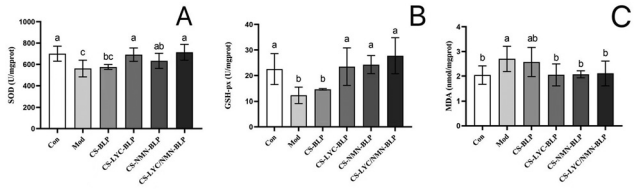

Fig. 7 Levels of oxidative stress in the liver. (A) Activity of SOD in the liver. (B) Activity of GSH-px in the liver. (C) Content of MDA in the liver. No significant difference between groups is represented by the same letter ($P > 0.05$), and significant difference is represented by different letters ($P < 0.05$). Note: CS-BLP: chitosan and proanthocyanidins from Bayberry leaves, CS-LYC-BLP: lycopene-loaded microgel, CS-NMN-BLP: nicotinamide mononucleotide-loaded microgel, CS-LYC/NMN-BLP: lycopene and nicotinamide mononucleotide co-loaded microgel.

induced oxidative stress in the liver (Fig. 7). Compared with the control group, the model and CS-BLP groups showed a significant decrease in SOD and GSH-px activities and a significant increase in MDA content ($P < 0.05$). Compared with those of the LPS group, the activity of antioxidant enzymes obviously increased and the MDA content significantly decreased after LYC and NMN pretreatment ($P < 0.05$).

Liver H&E staining

Whether the histological changes in the liver differed among groups was further investigated with H&E staining. As shown in Fig. 8, the hepatocytes in the control group were intact, whereas hepatocyte necrosis, inflammatory cell infiltration, and vacuolar degeneration were observed in the model group (arrow points). The other groups, especially the CS-LYC-BLP group, CS-NMN-BLP, and CS-LYC/NMN-BLP groups, showed significant improvement in the above liver histological changes.

Significantly modulated inflammatory response and oxidative stress signaling pathways in the liver by microgels loaded with LYC and NMN

TLR4/NF-κB and Sirt1/Nrf2 signaling pathways were analyzed to explore the underlying molecular mechanisms by which

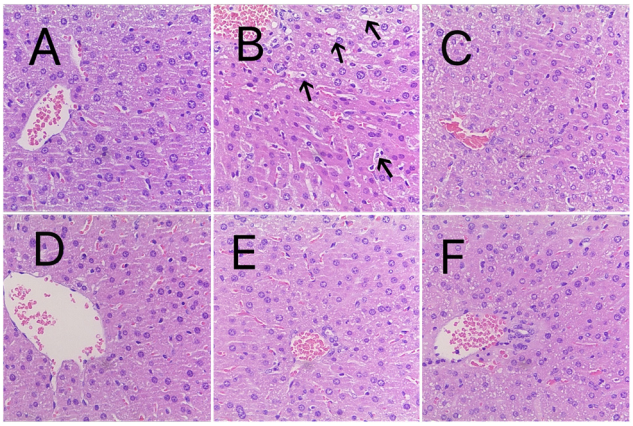

Fig. 8 Morphological changes in the livers of mice (H&E staining, ×200). (A) The control group, (B) model group, (C) CS-BLP group, (D) CS-LYC-BLP group, (E) CS-NMN-BLP group and (F) CS-LYC/NMN-BLP group.

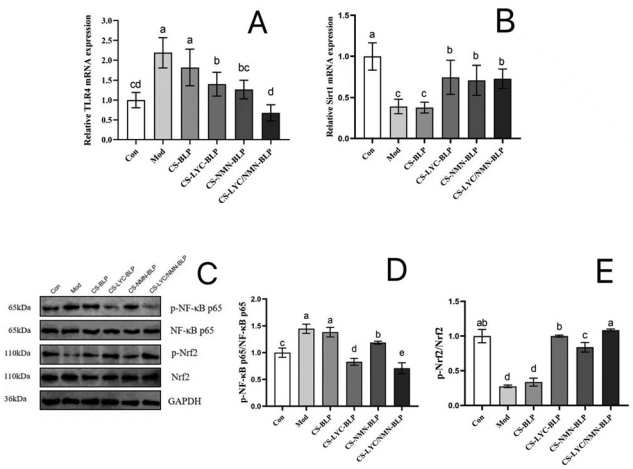

Fig. 9 Effects of LYC and NMN on the inflammatory response and oxidative stress signaling pathways in the liver. (A) Relative TLR4 mRNA expression. (B) Relative Sirt1 mRNA expression. (C) The image of western blotting. (D) The activation of NF-κB. (E) The activation of Nrf2. No significant difference between groups represented by the same letter ($P > 0.05$), but significant difference by different letters ($P < 0.05$). Note: CS-BLP: chitosan and proanthocyanidins from Bayberry leaves, CS-LYC-BLP: lycopene-loaded microgel, CS-NMN-BLP: nicotinamide mononucleotide-loaded microgel, CS-LYC/NMN-BLP: lycopene and nicotinamide mononucleotide co-loaded microgel.

LYC and NMN mitigate LPS-induced liver inflammation. The relative mRNA levels of TLR4 (Fig. 9A) and Sirt1 (Fig. 9B) in the liver were detected by RT-qPCR. LPS administration upregulated the hepatic mRNA level of TLR4 and downregulated the Sitr1 mRNA level drastically compared with the control ($P < 0.05$). Compared with the model group, the CS-LYC-BLP, CS-NMN-BLP, and CS-LYC/NMN-BLP groups demonstrated a significant decrease in the hepatic mRNA level of TLR4 and a significant increase in the Sirt1 level ($P < 0.05$). Moreover, the synergistic effect of LYC and NMN was significantly exhibited by inhibiting the TLR4 transcription level ($P < 0.05$).

The activation of NF-κB and Nrf2 is shown in Fig. 9C–E. Compared with the control group, the model and CS-BLP groups had significantly upregulated values of p-NF-κB p65/NF-κB p65 and significantly downregulated values of p-Nrf2/Nrf2 ($P < 0.05$), indicating that LPS promoted the activation of NF-κB and inhibited Nrf2. The phosphorylation level of NF-κB p65 in the CS-LYC-BLP, CS-NMN-BLP, and CS-LYC/NMN-BLP groups significantly decreased, whereas the phosphorylation level of Nrf2 significantly increased compared with those in the model group ($P < 0.05$). In particular, the phosphorylation of NF-κB p65 and Nrf2 was more significant when LYC and NMN acted together ($P < 0.05$).

Identification of serum EVs

As shown in the TEM observation in Fig. 10A, the EVs had a saucer-like shape, and the particle sizes in all groups were distributed in the range of 50–120 nm (Fig. 10B). The marker proteins CD9, CD63, and TSG101 were detected for EV characterization (Fig. 10C).

Significantly regulated miRNA level in serum EVs by microgels loaded with LYC and NMN

As shown in Fig. 11, compared with the model group, the other groups showed significantly increased expression levels of miR-145a-5p and miR-217-5p ($P < 0.05$). The expression in the CS-LYC/NMN-BLP group was the highest. According to the RT-qPCR results of TLR4 and bioinformatics analysis in the TargetScan and miRDB databases, the expression levels of miRNAs, especially miR-217-5p, may be strongly associated with the TLR4 mRNA levels.

In vitro interaction of miR-217-5p with TLR4 mRNA

The RT-qPCR results elucidated that the expression levels of miR-217-5p in the serum EVs significantly differed among the groups and showed negative correlation with the levels of

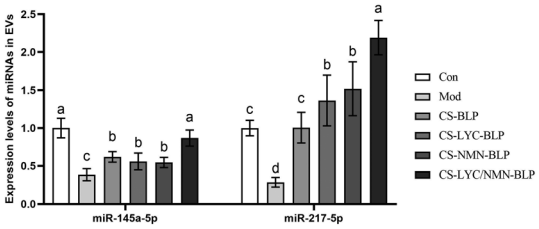

Fig. 11 MiRNA expression of EVs. No significant difference between groups is represented by the same letter ($P > 0.05$), and significant difference is represented by different letters ($P < 0.05$). Note: CS-BLP: chitosan and proanthocyanidins from Bayberry leaves, CS-LYC-BLP: lycopene-loaded microgel, CS-NMN-BLP: nicotinamide mononucleotide-loaded microgel, CS-LYC/NMN-BLP: lycopene and nicotinamide mononucleotide co-loaded microgel.

TLR4 mRNA. The interactions of miR-217-5p and TLR4 mRNA were further tested by constructing reporter plasmids of the potential action points of TLR4 mRNA and conducting a dual-luciferase reporter assay (Fig. 12A). As shown in Fig. 12B, the relative fluorescence value of the mmu-miR-217-5p + TLR4-WT co-transfection group was lower ($P < 0.05$) than that of the miR-NC + TLR4-WT co-transfection group. After TLR4 mRNA mutation, no difference in the relative fluorescence value was observed between the co-transfection of miR-NC + TLR4 and mmu-miR-217-5p + TLR4 groups ($P > 0.05$). The above results implied the existence of interaction sites for miR-217-5p and its respective target mRNAs, TLR4. These sites may be the key to relieve inflammation by a post-transcription mechanism between miRNAs and mRNAs.

LYC and NMN interactions with TLR4/MD2 complexes

The molecular docking results showed that the optimal binding energy of NAD+ and the TLR4/MD2 complex was −5.13 kcal mol^{-1}, and the binding site was on the structure of TLR4. It was predicted that NAD+ was able to interact with TLR4 residues Ile218, Ser240, Arg268, Lys239, and Asn216, with four predicted hydrogen bonds between NAD+ and TLR4 residues Lys239 and Arg268 (Fig. 13A). Meanwhile, the optimal binding energy of LYC and the TLR4/MD2 complex was

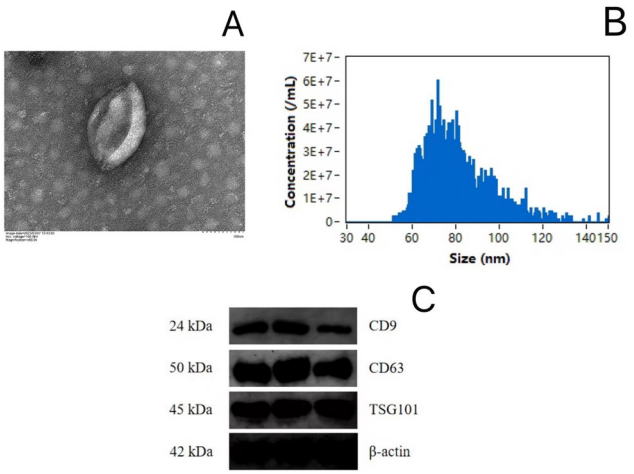

Fig. 10 Identification of serum extracellular vehicles. (A) Serum EVs observed by transmission electron microscopy (TEM) at the scale of 100 nm. (B) Particle size analysis. (C) Expression levels of CD9, CD63, and TSG101 determined by western blotting.

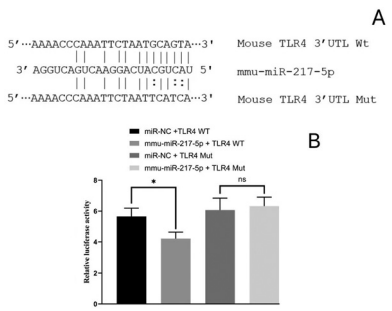

Fig. 12 TLR4 is a molecular target of miR-217-5p. (A) The alignment of miR-217-5p and TLR4 3′-UTR by computational prediction using TargetScan and miRanda. (B) The dual–luciferase reporter assay was performed in 293T cells. *$P < 0.05$.

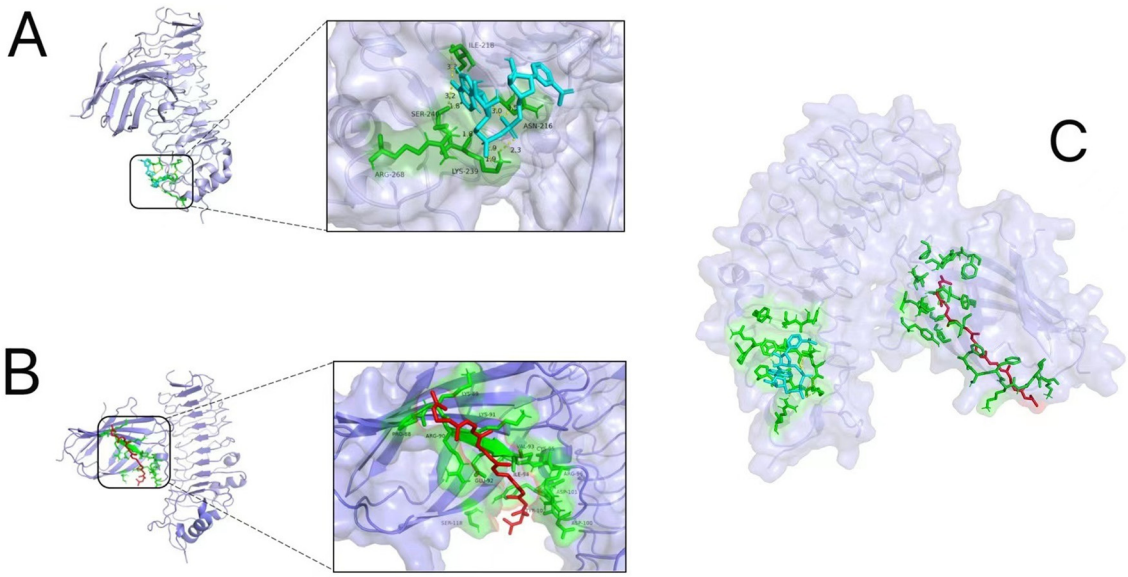

Fig. 13 Results of molecular docking. (A) NAD+ interaction with the TLR4/MD2 complex; (B) LYC interaction with the TLR4/MD2 complex; and (C) LYC and NAD+ interaction with the TLR4/MD2 complex.

−8.01 kcal mol^{-1}, and its binding site was in the hydrophobic cavity of MD2, which suggested that an interaction existed between LYC and MD2 residues Lys89, Lys91, Pro88, Arg90, Glu92, Ser118, Tyr102, Asp100, Asp101, Cys95, Arg96, and Val93 (Fig. 13B). The binding energy in molecular docking can evaluate the strength of the interaction between small molecules and proteins. A binding energy below −5 kcal mol^{-1} indicates good binding. The results indicated that LYC and NMN can spontaneously bind to the TLR4/MD2 complex, with good binding activity and no competitive binding. In addition, docking NAD+ to TLR4/MD2 and then docking LYC to the TLR4/MD2/NAD+ complex was feasible, because the binding energy was −6.89 kcal mol^{-1}, which can help in binding spontaneously and resulted in good binding activity (Fig. 13C). These results indicated that LYC and NMN could interact together with the TLR4/MD2 complex, thereby inhibiting the downstream NF-κB pathway activation and reducing the inflammatory response.

Significantly ameliorated composition and diversity of the gut microbiota in LPS-induced mice by microgels loaded with LYC and NMN

16S rRNA sequencing analysis was performed to explicate the influence of LYC and NMN on the gut microbiota diversity and abundance in LPS-treated mice. Analysis of the species accumulation curves (Fig. 14A) showed that the curve tended to be stable, indicating that the sample was sufficiently large to show species richness. Chao, Shannon, and Simpson indices were used to assess microbial diversity within individual samples, and no significant differences were found between groups (Fig. 14B). Principal coordinate analysis (PCoA) was used to assess the β diversity of the gut microbiota (Fig. 14C). PC1 and PC3 accounted for 30.09% and 7.75% of the total analysis data, respectively. After LPS induction, the model and control groups were obviously separated. Based on PC1, the composition structure of the gut microbiota in the CS-BLP and CS-LYC-BLP groups was not significantly different from that of the model group, whereas those of the CS-NMN-BLP and CS-LYC/NMN-BLP groups were closer to that of the control group.

The relative abundance of the gut microbiota was analyzed at the phylum level. *Firmicutes* and *Bacteroidetes* were found to be the primary phyla of the gut microbiota. After LPS induction, the abundance of *Firmicutes* decreased, whereas that of *Bacteroidetes* increased, and the ratio of *Firmicutes* and *Bacteroidetes* (F/B) decreased. However, the F/B ratio increased after the intervention of microgels loaded with LYC or NMN. Linear discriminant analysis effect size (LEfSe) was calculated to identify the statistically dominant microbiota among these groups. *Enterorhabdus* and *Bilophila* were the dominant genera in the LPS group ($P < 0.05$), but they returned to normal levels after the intervention of microgels loaded with LYC or NMN. In addition, *Helicobacter*, *Escherichia Shigella*, *Eubacterium fissicatena*, *Streptococcus*, *Proteus*, and *Butyricimonas* were the dominant genera in the CS-BLP group. *Acinetobacter*, *Roseburia*, *Exiguobacterium*, *Corynebacterium 1*, and *Kurthia* were significantly enriched in the CS-LYC-BLP group. The *Ruminococcus torques* group and *Clostridium innocuum* group were confirmed to be the dominant genera in the CS-NMN-BLP group. Meanwhile, CS-LYC/NMN-BLP significantly enriched *Paraprevotella* and *Rikenellaceae RC9* gut group (Fig. 14D–G).

Discussion

Microgels composed of edible natural polymers not only can protect and target bioactive substances but also have the

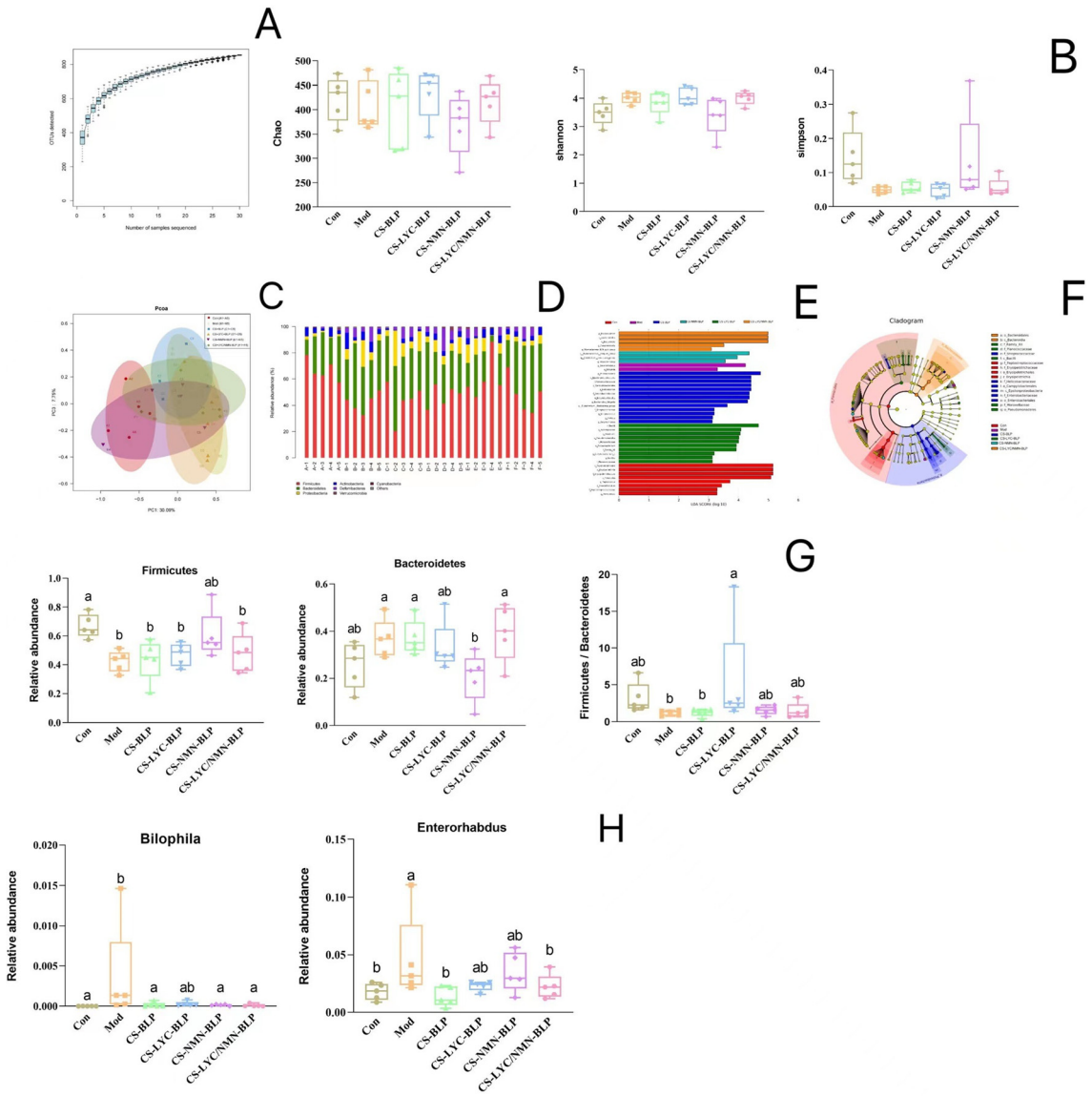

Fig. 14 Microgels loaded with LYC and NMN altered the composition and diversity of the gut microbiota in LPS-induced mice. (A) OTU sparsity curves. (B) α-Diversity index (observed, Chao1, Shannon, and Simpson indices). (C) The Bray–Curtis PCoA plot based on the OTU abundance of each mouse. (D) Heat map of bacterial taxonomic profiling at the phylum level of intestinal bacteria based on each rat from different groups: control group (A1–A5), model group (B1–B5), CS-BLP group (C1–C5), CS-LYC-BLP group (D1–D5), CS-NMN-BLP group (E1–E5), and CS-LYC/NMN-BLP group (F1–F5). (E) Linear discriminant analysis (LDA) scores. (F) Cladogram generated from linear discriminate analysis effect size (LEfSe) analysis. (G) The relative abundance of gut microbiota at the phylum level. (H) The relative abundance of gut microbiota at the genus level. No significant difference between groups represented by the same letter ($P > 0.05$), but significant difference by different letters ($P < 0.05$).

advantages of safety, nontoxicity, and good biocompatibility. Previous studies[16,24] showed that crosslinking between CS and proanthocyanidins can occur through hydrogen bonding and electrostatic interactions. In the present study, LYC liposomes and NMN were encapsulated by microgels prepared by CS and BLP, and a system of co-existence of fat-soluble and water-soluble substances was constructed. The microgels improved the stability of LYC and NMN under various influencing factors. In simulated digestion, the microgels can avoid the degradation of LYC and NMN by stomach acid and successively target their release in the intestine. In addition, liposomes and a phospholipid bilayer with a similar structure of bio-membrane can fuse with each other to promote the absorption of functional factors.[25] CS is able to adsorb with the cell membrane through electrostatic interactions and activate ion channels and the corresponding protein transporters to increase the transmembrane absorption of functional factors.[14] Therefore, microgels could achieve more efficient absorption of LYC and NMN and achieve long-term lasting effects. The bioavailability of lycopene is low, and it loses its activity after metabolism. Some studies have used different encapsulation systems to protect lycopene and ameliorate its stability.[26] NMN

has low bioavailability, and its metabolite nicotinamide is highly active,[27] while nicotinamide is poorly absorbed and metabolized quickly.[28,29] Therefore, protecting the stability of NMN in the digestive tract and improving its bioavailability are capable of maximizing its activity.

LPS, as an important component of the outer membrane of cell wall from Gram-negative bacteria, can cause many diseases. In daily life, stimulation by bad diet, drugs, or other bacterial infections can disrupt the homeostasis of the intestinal flora, causing damage to the intestinal mucosal barrier and bacterial translocation. A large amount of endotoxin leaks from the intestine through the portal vein into the liver, causing oxidative stress and inflammatory reactions, and ultimately liver tissue damage.[1] Considering the liver serves as the core organ of immune homeostasis and metabolism, the research for function factors that are effective in preventing acute liver injury has become critical. The present study showed that LYC and NMN significantly protected mice against LPS-induced acute liver injury by co-inhibiting the TLR4/NF-κB and Sirt1/Nrf2 signaling pathways.

When the body fails to remove a large number of free radicals and peroxides stimulated by LPS in cells or tissues in a timely manner, the homeostasis between oxidation and antioxidation in the body immediately induces cell necrosis or apoptosis, resulting in tissue damage.[30] Lipid peroxidation is a clear mechanism that causes animal cell damage. As an end product of membrane lipid peroxidation, MDA can damage the structure and function of proteins by forming a stable adduct, and it is used as a marker of oxidative stress.[31] SOD and GSH-px are important contributors to maintaining intracellular REDOX balance and can improve the body's antioxidant capacity.[32] Consistent with previous reports,[22] LPS stimulation increased the MDA content in the liver and inhibited the activity of antioxidant enzymes, resulting in the accumulation of lipid peroxides and oxidative stress in the liver. LYC and NMN can restore the activity of antioxidant enzymes and inhibit further oxidation of excess lipid peroxides. Nrf2 is a transcription factor that plays a crucial role in enhancing cellular protection against oxidative damage. Nrf2 is normally coupled to Keap1 and present in the cytoplasm in an inactive form. However, under the stimulation of LPS, Nrf2 is phosphorylated and separated from Keap1 and translocated to the nucleus, binds to antioxidant reaction elements and promotes its related targets, regulates a series of antioxidant enzymes, and thus achieves the role of anti-oxidative stress damage. Studies showed that Sirt1 can dissociate Nrf2 and promote its activation and nuclear translocation by changing the configuration of Keap1.[33] Activation can also be achieved by directly promoting the deacetylation of Nrf2.[34] In the present study, LPS inhibited the transcription of Sirt1, thereby inhibiting the activation of Nrf2 and resulting in a decrease in the antioxidant capacity of the system, which cannot remove free radicals and peroxides in time. This phenomenon resulted in oxidative damage, which also explained the decreased activity of antioxidant enzymes and the accumulation of MDA in the livers of mice. LYC and NMN promoted Nrf2 phosphorylation activation and nuclear translocation by upregulating the transcription level of Sirt1, thus improving the antioxidant capacity of the body.

Oxidative stress is closely related to inflammation, which stimulates cells to release ROS and thus aggravates oxidative stress. Oxidative stress and inflammation can cause more serious damage by interacting and amplifying each other's damage. TNF-α, IL-6, and IL-1β are important pro-inflammatory factors in the inflammatory response. TNF-α can induce the production of other inflammatory factors or adhesion molecules.[35] IL-6 can synergistically cascade with other inflammatory cytokines to promote and amplify the inflammatory response.[36] In addition, IL-1β can stimulate antigen-presenting cells and indirectly promote neutrophils to reach inflammatory sites and release oxygen free radicals and lysosomal enzymes.[37] LPS stimulation can increase the level of inflammatory factors in serum, thus causing systemic inflammation.[38] The same result was obtained in the present study.

TLR4 is LPS-specific recognition receptor that binds to activate by LPS. When LPS enters the cell, its lipid A structure is recognized by an LPS-binding protein and forms a CD14-LPS complex with its receptor (CD14). Subsequently, the CD14-LPS complex, together with myeloid differentiation protein 2 (MD2), a key adaptor of the TLR4 signaling pathway, promotes the activation of TLR4 to form the TLR4/MD2/LPS complex, which triggers the innate immune response and inflammatory cascade.[39] NF-κB p65 is an evolutionarily conserved transcription factor that is normally bound by kappa B (IκB) and exists in an inactive form in the cytoplasm. Upon stimulation by LPS; NF-κB p65 dissociates and phosphorylates IκB, transfers from the cytoplasm to the nucleus, transcribes genes encoding pro-inflammatory mediators, and ultimately promotes the production of inflammatory factors, ROS, and active nitrogen.[40] The three main methods to inhibit the overactivation of the TLR4 signaling pathway include downregulation of TLR4 expression, direct binding to TLR4 or the TLR4/MD2 complex to inhibit TLR4 activity, and direct binding to MD2 to inhibit the TLR4 signaling pathway.[41] The present study found that LYC and NMN intervention can co-downregulate TLR4 mRNA levels. Molecular docking was used to simulate the interaction of LYC and NAD^+ on the TLR4/MD2 complex to further understand the co-inhibition mechanism of LYC and NMN on the TLR4 pathway. LYC and NMN were able to bind uncompetitively to different sites of the TLR4/MD2 complex, inhibiting TLR4 activity and thereby preventing downstream NF-κB p65 activation. Consequently, the secretion of inflammatory factors was inhibited, and the inflammatory response was reduced.

MiRNAs are important endogenous short-strand noncoding RNAs involved in transcription and post-transcriptional regulation. Studies showed that miRNAs are abundant, sensitive, and efficient *in vivo*, and they can be used as a new class of immune regulatory factors to bind to target genes through special sequences, inhibit gene expression, and participate in the regulation of the innate immune response and inflammatory response. Previous studies reported that miR-217-5p can not only inhibit cell damage and reduce the production of pro-

inflammatory factors by targeting YY1 associated factor 2,[42] but also inhibit the expression of NF-κB to reduce the inflammatory response.[43] Although some of the molecular targets are unknown, miR-217-5p can undeniably inhibit the inflammatory response. However, whether miR-217-5p plays an anti-inflammatory role in the LPS-induced inflammatory response remains unclear. Therefore, the possible role of miR-217-5p in LPS-induced inflammatory responses was elucidated in the present study by using LPS-induced liver injury in mice. The detection results showed that the expression of miR-217-5p was significantly different among the six groups and negatively correlated with the expression of TLR4. The dual luciferase reporter gene assay confirmed a significant interaction between miR-217-5p and TLR4. Therefore, the mitigation mechanism of LYC and NMN microgels on LPS-induced liver inflammation may be related to the regulation of miRNA signaling pathways.

The liver is closely related to the intestinal flora, and its health cannot be separated from the balance of the intestinal flora. Ecological imbalance of the intestinal flora could affect immune homeostasis, thus leading to the inflammatory response of the body.[44] Although the gut microbiota can regulate the immune system by releasing LPS, excessive LPS levels can disrupt its homeostasis.[45] According to the PCoA results, LPS stimulation significantly changed the composition of the intestinal flora. Firmicutes is an important indicator of intestinal health,[46] and an increased relative abundance of Proteobacteria may induce inflammatory responses.[47] Therefore, the F/B ratio is an important parameter to measure the homeostasis of the intestinal flora. After LPS stimulation, the F/B ratio decreased, indicating that the inflammatory response destroyed the homeostasis of the body's intestinal environment, consistent with the findings of Wang *et al.*[48] LEfSe analysis showed that the dominant bacteria in the LPS group were *Bilophila* and *Enterorhabdus*, which were closely related to inflammation.[49,50] In the study of Xia *et al.*,[49] *Bilophila* was confirmed to be positively correlated with inflammatory proteins, oxidative stress parameters, and TLR4 in the liver, consistent with the results obtained in the present study. In addition, *Roseburia*,[51] *Ruminococcus torques* group,[52] and *Rikenellaceae RC9* gut group,[53] as probiotics that can produce short-chain fatty acids, can protect the body against pathogens and diseases; they were enriched in the CS-LYC-BLP, CS-NMN-BLP, and CS-LYC/NMN-BLP groups, respectively. In other words, the intervention of LYC and NMN inhibited the infection and reproduction of harmful bacteria and enriched the intestinal probiotic flora.

Conclusions

Overall, the packaging of LYC and NMN in microgels improved their stability and targeted release in the small intestine, alleviating LPS-induced oxidative stress and inflammation by regulating the TLR4/NF-κB and Sirt1/Nrf2 signaling pathways and the intestinal flora. This study has a certain reference value for the development of food additives and the mechanistic study of functional factors.

Author contributions

Jian Ge designed the experimental scheme, performed the experiment operation, and analyzed the data. Luting Ye and Min Cheng completed some experiments including the oral administration and collection of samples of the rats, and then writing and editing. Weijia Xu and Zhaowen Chen also provided some guidance and completed parts of the experiments. Feng Guan guided and supervised the whole experimental process.

Data availability

The dataset used and/or analyzed during the current research period can be obtained from the corresponding authors upon reasonable request.

Conflicts of interest

All authors declare that they have known competing financial interests or personal relationships that could have appeared to influence the work reported in this paper.

Acknowledgements

We are grateful to Zonghua Dong, Shengnan Zhu, Simin Ren and Xuanxuan Zou (College of Life Sciences, China Jiliang University) for generously providing facilities for mouse administration. We are sincerely thankful for the financial assistance from the National Natural Science Foundation of China and the Major Science and Technology Projects in Zhejiang Province.

References

1 K. Michael and C. Hans, Reparative inflammation takes charge of tissue regeneration, *Nature*, 2016, **529**, 307–315.
2 X. Y. Zhang, M. Wu, Y. M. Li, J. Yin, Y. B. Ji, H. Y. Liu and X. Zheng, Research progress on the effect and mechanism of lipopolysaccharide, *Adv. Vet. Sci.*, 2015, **36**, 133–136.
3 C. G. Corrêa, S. R. Miguel and C. Marlus, An Overview of Properties and Analytical Methods for Lycopene in Organic Nanocarriers, *Crit. Rev. Anal. Chem.*, 2020, **51**, 1–13.
4 Y. J. Tian, W. Q. Zhao, Z. Q. Xing, J. Zhang, H. W. Wang and Y. T. Zhang, Research progress on health care efficacy of lycopene, *Mod. Food*, 2022, **28**, 11–17.
5 S. A. Rajput, S. J. Liang, X. Q. Wang and H. C. Yan, Lycopene Protects Intestinal Epithelium from

Deoxynivalenol-Induced Oxidative Damage via Regulating Keap1/Nrf2 Signaling, *Antioxidants*, 2021, **10**, 1493.

6 J. Dong, W. Li, L. M. Cheng and G. G. Wang, Lycopene attenuates LPS-induced liver injury by inactivation of NF-κB/COX-2 signaling, *Int. J. Clin. Exp. Pathol.*, 2019, **12**, 817–825.

7 X. P. Liang, C. C. Ma, X. J. Yan, X. B. Liu and F. G. Liu, Advances in research on bioactivity, metabolism, stability and delivery systems of lycopene, *Trends Food Sci. Technol.*, 2019, **93**, 185–196.

8 W. Q. Hong, F. Mo, Z. Q. Zhang, M. Y. Huang and X. W. Wei, Nicotinamide Mononucleotide: A Promising Molecule for Therapy of Diverse Diseases by Targeting NAD+ Metabolism, *Front. Cell Dev. Biol.*, 2020, **8**, 246.

9 T. Laszlo and A. V. Vera, Generation of reactive oxygen species in the reaction catalyzed by alpha-ketoglutarate dehydrogenase, *J. Neurosci.*, 2004, **24**, 7771–7778.

10 N. E. Picciotto, L. B. Gano, L. C. Johnson, C. R. Martens, A. L. Sindler, K. F. Mills, S. I. Imai and D. R. Seals, Nicotinamide mononucleotide supplementation reverses vascular dysfunction and oxidative stress with aging in mice, *Aging cell*, 2016, **15**, 522–530.

11 R. ZapataPérez, A. Tammaro, B. V. Schomakers, A. M. L. Scantlebery, S. Denis, H. L. Elfrink, J. GiroudGerbetant, C. Cantó, C. LópezLeonardo, R. L. McIntyre, M. Weeghel, A. SánchezFerrer and R. H. Houtkooper, Reduced nicotinamide mononucleotide is a new and potent NAD+ precursor in mammalian cells and mice, *FASEB J.*, 2021, **35**, 1–17.

12 H. Q. Chen, D. Chou, H. X. Zheng, Y. X. Gao and L. K. Mao, Preparation, characterization and application of food microgels, *Chin. Food Addit.*, 2019, **30**, 171–180.

13 Y. Fu, L. P. Qiao, Y. M. Cao, X. Z. Zhou, Y. Liu and X. Q. Ye, Structural elucidation and antioxidant activities of proanthocyanidins from Chinese bayberry (Myrica rubra Sieb. et Zucc.) leaves, *PLoS One*, 2017, **9**, 1–12.

14 X. Y. Yuan, H. H. Xu, F. P. Shao, D. K. Yin and Y. Yang, Effect of chitosan nanoparticles on the transport of berberine through Caco-2 cell monolayers, *Chin. J. New Drugs*, 2018, **27**, 708–713.

15 Y. S. Zhao, Z. Xin, N. Li, S. Y. Chang, Y. D. Chen, L. Geng, H. R. Chang, H. L. Shi and Y. Z. Chang, Nano-liposomes of lycopene reduces ischemic brain damage in rodents by regulating iron metabolism, *Free Radicals Biol. Med.*, 2018, **124**, 1–11.

16 A. V. Emilia, E. A. Daniel, M. C. Sergio, G. K. Christian and D. R. Jess, Antimicrobial proanthocyanidin-chitosan composite nanoparticles loaded with gentamicin, *Int. J. Biol. Macromol.*, 2020, **162**, 1500–1508.

17 H. X. Liu, Q. R. Sun, W. H. Xiong and L. F. Zhang, Preparation of lycopene nanostructured liposomes, *China Oils Fats (Zhongguo Youzhi)*, 2018, **43**, 65–69.

18 L. Zhao, X. L. Zhang, J. M. Hu and C. T. Wang, Lycopene micelles prepared by soybean protein isolate combined with sodium alginate, *Food Sci.*, 2016, **37**, 1–6.

19 J. Xue, C. Tan, X. M. Zhang, B. Feng and S. Q. Xia, Fabrication of epigallocatechin-3-gallate nanocarrier based on glycosylated casein: stability and interaction mechanism, *J. Agric. Food Chem.*, 2014, **62**, 4677–4684.

20 Y. P. Li, X. Pan, M. Y. Yin, C. P. Li and L. R. Han, Preventive Effect of Lycopene in Dextran Sulfate Sodium-Induced Ulcerative Colitis Mice through the Regulation of TLR4/TRIF/NF-κB Signaling Pathway and Tight Junctions, *J. Agric. Food Chem.*, 2021, **69**, 13500–13509.

21 F. Pan, S. F. Kang, Y. F. Zhao, L. Dai, Q. Shao, Y. Yang, Q. K. Chen, J. J. Zhu and L. F. Cui, Effect of beta-nicotinamide mononucleotide on tumor formation and growth in a lung cancer mouse model, *Mater. Chem. Front.*, 2021, **5**, 995–1002.

22 L. Du, Y. Zheng, Y. H. Yang, Y. J. Huang, Y. M. Hao, C. Chen, B. Z. Wang, X. Guo, H. Wu and G. H. Su, Krill oil prevents lipopolysaccharide-evoked acute liver injury in mice through inhibition of oxidative stress and inflammation, *Food Funct.*, 2022, **13**, 3853–3864.

23 X. Chen, J. W. Yu, L. F. Zheng, Z. Y. Deng and H. Y. Li, Quercetin and lycopene co-administration prevents oxidative damage induced by d-galactose in mice, *Food Biosci.*, 2022, **50**, 12042–12052.

24 Y. M. He, S. Guo, R. Chang, D. Zhang, Y. K. Ren, F. X. Guan and M. H. Yao, Facile preparation of antibacterial hydrogel with multi-functions based on carboxymethyl chitosan and oligomeric procyanidin, *RSC Adv.*, 2022, **12**, 20897–20905.

25 G. Bozzuto and A. Molinari, Liposomes as nanomedical devices, *Int. J. Nanomed.*, 2015, **10**, 975–999.

26 Y. D. Sun, M. M. Zhong, Y. F. Sun, Y. Li, B. K. Qi and L. Z. Jiang, Stability and digestibility of encapsulated lycopene in different emulsion systems stabilized by acid-modified soybean lipophilic protein, *J. Sci. Food Agric.*, 2022, **102**(13), 6146–6155.

27 M. Ru, W. W. Wang, Z. Y. Zhai, R. X. Wang, Y. M. Li, J. Liang, D. Kothari, K. M. Niu and X. Wu, Nicotinamide mononucleotide supplementation protects the intestinal function in aging mice and D-galactose induced senescent cells, *Food Funct.*, 2022, **13**(14), 7507–7519.

28 C. J. Gross and L. M. Henderson, Digestion and absorption of NAD by the small intestine of the rat, *J. Nutr.*, 1983, **113**(2), 412–420.

29 S. A. Schuette and R. C. Rose, Nicotinamide uptake and metabolism by chick intestine, *Am. J. Physiol.*, 1983, **245**(4), G531–G538.

30 L. Du, Y. M. Hao, Y. H. Yang, Y. Zheng, Z. J. Wu, M. Q. Zhou, B. Z. Wang, Y. M. Wang, H. Wu and G. H. Su, DHA-Enriched Phospholipids and EPA-Enriched Phospholipids Alleviate Lipopolysaccharide-Induced Intestinal Barrier Injury in Mice via a Sirtuin 1-Dependent Mechanism, *J. Agric. Food Chem.*, 2022, **70**, 2911–2922.

31 H. J. Zhang, S. S. Zhang, J. Wang and B. G. Sun, Wheat bran feruloyl oligosaccharides protect against AAPH-induced oxidative injury via p38MAPK/PI3K-Nrf2/Keap1-MafK pathway, *J. Funct. Foods*, 2017, **29**, 53–59.

32 M. VillanuevaPaz, L. Morán, N. LópezAlcántara, C. Freixo, R. J. Andrade, M. I. Lucena and F. J. Cubero, Oxidative Stress in Drug-Induced Liver Injury (DILI): From Mechanisms to Biomarkers for Use in Clinical Practice, *Antioxidants*, 2021, **10**, 390.

33 W. Tang, Y. F. Jiang, M. Ponnusamy and M. Diallo, Role of Nrf2 in chronic liver disease, *World J. Gastroenterol.*, 2014, **20**, 13079–13087.

34 B. Y. Yao, J. N. He, X. Yin, Y. Shi, J. Wan and Z. Tian, The protective effect of lithocholic acid on the intestinal epithelial barrier is mediated by the vitamin D receptor via a SIRT1/Nrf2 and NF-κB dependent mechanism in Caco-2 cells, *Toxicol. Lett.*, 2019, **316**, 109–118.

35 T. Jiang, J. Zhou, W. Liu, W. Tao, J. R. He, W. P. Jin, H. Guo, N. Yang and Y. B. Li, The anti-inflammatory potential of protein-bound anthocyanin compounds from purple sweet potato in LPS-induced RAW264.7 macrophages, *Food Res. Int.*, 2020, **137**, 1–11.

36 H. Yamanaka, TNF as a Target of Inflammation in Rheumatoid Arthritis, *Endocr., Metab. Immune Disord.: Drug Targets*, 2015, **15**, 129–134.

37 S. R. Planck, A. Woods, J. S. Clowers, M. J. Nicklin, J. T. Rosenbaum and H. L. Rosenzweig, Impact of IL-1 signalling on experimental uveitis and arthritis, *Ann. Rheum. Dis.*, 2012, **71**, 753–760.

38 Y. Qiao, X. F. Bai and Y. G. Du, Chitosan oligosaccharides protect mice from LPS challenge by attenuation of inflammation and oxidative stress, *Int. Immunopharmacol.*, 2010, **11**, 121–127.

39 C. Whitfield and M. S. Trent, Biosynthesis and Export of Bacterial Lipopolysaccharides, *Annu. Rev. Biochem.*, 2014, **83**, 99–128.

40 M. Gasparrini, H. T. Y. Forbes, D. Cianciosi, J. L. Quiles, B. Mezzetti, J. B. Xiao, F. Giampieri and M. Battino, The efficacy of berries against lipopolysaccharide-induced inflammation: A review, *Trends Food Sci. Technol.*, 2021, **117**, 74–91.

41 Y. S. Zhang, X. J. Liang, X. F. Bao, W. Xiao and G. L. Chen, Toll-like receptor 4 (TLR4) inhibitors: Current research and prospective, *Eur. J. Med. Chem.*, 2022, **235**, 1–20.

42 X. H. Wang, J. Qian, Y. Meng, P. Wang, R. Z. Cheng, G. X. Zhou, S. X. Zhu and C. Liu, Salidroside alleviates severe acute pancreatitis-triggered pancreatic injury and inflammation by regulating miR-217–5p/YAF2 axis, *Int. Immunopharmacol.*, 2022, **111**, 109123.

43 L. X. Yang, S. Liu, L. Yang, B. Xu, M. Q. Wang, X. S. Kong and Z. C. Song, miR-217–5p suppresses epithelial-mesenchymal transition and the NF-κB signaling pathway in breast cancer via targeting of metadherin, *Oncol. Lett.*, 2022, **23**, 162.

44 J. Sun, H. Chen, J. Kan, Y. R. Gou, J. Liu, X. Zhang, X. N. Wu, S. X. Tang, R. Sun, C. L. Qian, N. F. Zhang, F. X. Niu and C. H. Jin, Anti-inflammatory properties and gut microbiota modulation of an alkali-soluble polysaccharide from purple sweet potato in DSS-induced colitis mice, *Int. J. Biol. Macromol.*, 2020, **153**, 708–722.

45 L. Annegret, B. Josef, Z. Qendrim and M. Z. Barbara, Dietary Deoxynivalenol Contamination and Oral Lipopolysaccharide Challenge Alters the Cecal Microbiota of Broiler Chickens, *Front. Microbiol.*, 2018, **9**, 804.

46 H. Q. Li, Y. Zhou, H. Y. Ling, L. Luo, D. S. Qi and L. Feng, The effect of dietary supplementation with Clostridium butyricum on the growth performance, immunity, intestinal microbiota and disease resistance of tilapia (Oreochromis niloticus), *PLoS One*, 2019, **14**, 1–24.

47 M. I. M. L. Vasques, V. F. M. Silva, C. S. Miranda, C. E. C. B. Andrade, J. B. Daleprane and M. V. Souza, A rise in Proteobacteria is an indicator of gut-liver axis-mediated nonalcoholic fatty liver disease in high-fructose-fed adult mice, *Nutr. Res.*, 2021, **91**, 26–35.

48 P. H. Wang, Z. H. Feng, X. Sang, W. Z. Chen, X. N. Zhang, J. B. Xiao, Y. Q. Chen, Q. Chen, M. H. Yang and J. Q. Su, Kombucha ameliorates LPS-induced sepsis in a mouse model, *Food Funct.*, 2021, 10263–10280.

49 T. Xia, W. H. Duan, Z. J. Zhang, S. P. Li, Y. X. Zhao, B. B. Geng, Y. Zheng, J. W. Yu and M. Wang, Polyphenol-rich vinegar extract regulates intestinal microbiota and immunity and prevents alcohol-induced inflammation in mice, *Food Res. Int.*, 2021, **140**, 110064.

50 Y. Li, J. Qin, Y. H. Cheng, Z. Y. Han, M. Li, Y. X. Qi, Q. C. Zhao and Z. B. Li, Polysaccharide from Patinopecten yessoensis Skirt Boosts Immune Response via Modulation of Gut Microbiota and Short-Chain Fatty Acids Metabolism in Mice, *Foods*, 2021, **10**, 2–15.

51 Y. K. Liu, C. H. Nakatsu, J. H. Yava, K. Ariangela and J. Qing, Vitamin E alpha- and gamma-tocopherol mitigate colitis, protect intestinal barrier function and modulate the gut microbiota in mice, *Free Radicals Biol. Med.*, 2021, **163**, 180–189.

52 Y. S. Bai, K. D. Mai, J. B. Li, Z. S. Ren, J. Zhang and A. S. Shan, Lactobacillus rhamnosus GG ameliorates DON-induced intestinal damage depending on the enrichment of beneficial bacteria in weaned piglets, *J. Anim. Sci. Biotechnol.*, 2022, **13**, 2–17.

53 A. Li, J. X. Ding, T. Shen, Y. Liang, F. Wei, Y. Wu, M. Lqbal, M. F. Kulyar, K. Li and K. H. Wei, Radix paeoniae alba polysaccharide attenuates lipopolysaccharide-induced intestinal injury by regulating gut microbiota&#13, *Front. Microbiol.*, 2023, **13**, 1–13.

